Supporting Information

Accomplishment of Multi-Functional π-Conjugated Polymers by Regulating the Degree of Side-Chain Fluorination for Efficient Dopant-Free Ambient-Stable Perovskite Solar Cells and Organic Solar Cells

Kakaraparthi Kranthiraja,[†] Sang Ho Park,[†] Hyunji Kim,[†] Kumarasamy Gunasekar,[†] Gibok Han,[§] Bumjoon J. Kim,[§] Chang Su Kim,[‖] Soohyun Kim,[⊥] Hyunjung Lee,*[,⊥] Ryosuke Nishikubo,[#] Akinori Saeki,*[,#] Sung-Ho Jin,*[,†] Myungkwan Song,*[,‖]

[†]Department of Chemistry Education, Graduate Department of Chemical Materials, Institute for Plastic Information and Energy Materials, Pusan National University, Busan, 46241, Korea

[§]Department of Chemical and Biomolecular Engineering, Korea Advanced Institute of Science and Technology (KAIST), Daejeon, 305-701, Korea

[‖]Surface Technology Division, Korea Institute of Materials Science, Changwon 641-831, Korea

[⊥]School of Advanced Materials Engineering, Kookmin University, Seoul, 136–702, Korea

[#]Department of Applied Chemistry, Graduate School of Engineering, Osaka University, Osaka 565-0871, Japan

Corresponding Authors

*E-mail: hyunjung@kookmin.ac.kr (H. L.).

*E-mail: saeki@chem.eng.osaka-u.ac.jp (A. S.).

*E-mail: shjin@pusan.ac.kr (S.-H. J.).

*E-mail: smk1017@kims.re.kr (M. S.).

Experimental Section:

Materials and characterization. 2-Tributylstannylthiophene (97%), 4-bromo-2-fluorophenol (98%) were purchased from Alfa Aesar (Korea). 4,8-Dihydrobenzo[1,2-b:4,5-b]dithiophen-4,8-dione was purchased from Solarmer (China). Tris(dibenzylideneacetone) dipalladium (0) ($Pd_2(dba)_3$, 97%), tri(*o*-tolyl)phosphine ((*o*-tol)$_3$P, 97%) and tetrakis(triphenylphsophine)palladium (0) ($Pd(PPh_3)_4$, 99%), were purchased from Sigma Aldrich (Korea). Spiro-OMeTAD (99.5%), $PC_{71}BM$ were obtained from Lumtec (Taiwan) and Solemme BV (Netherlands) respectively. PEDOT:PSS (Clevios P VP AI 4083) obtained from Heraeus Deutschland GmbH & Co. KG (Germany). Titanium diisopropoxide dis(acetylacetonate) and $TiCl_4$ (98%) were obtained from Sigma Aldrich (Korea). Acetonitrile (99.8%), chlorobenzene (CB, 99.8%), diethyl ether (99.7%), DMF (99.8%) and DMSO (99.9%) were purchased from Sigma Aldrich (Korea).

^{1}H and ^{13}C NMR spectra were recorded on a Varian Mercury Plus 300 MHz spectrometer (USA) in $CDCl_3$ using tetramethylsilane (TMS) as an internal standard. IR spectra of P1-P3 were characterized from Agilent Cary 630 FTIR (USA). The UV-vis absorption spectra and emission spectra were recorded on a JASCO V-570 spectrophotometer (USA) and Hitachi F-4500 fluorescence spectrophotometer (Japan), respectively at room temperature. Thermal gravimetric analysis (TGA) and differential scanning calorimetry (DSC) were carried out on a Mettler Toledo TGA/SDTA 851e (Switzerland) under N_2 atmosphere at a heating rate of 10 °C/min. Stille polymerization reactions were conducted in microwave (CEM focused TM synthesis system, USA). The number-average and weight-average molecular weights (M_n and M_w) of P1-P3 were determined relative to a polystyrene standard with THF as the eluent at 25 ºC using gel permeation chromatography (Agilent GPC 1200 series, Germany). CV experiments were carried

out in acetonitrile (0.1 M solution of tetrabutylammonium perchlorate) at a scan rate of 100 mV/s using CHI 600C potentiostat (CH Instruments, Korea); three electrode cell systems with platinum, Ag/AgCl and platinum wire were used as the working, reference and counter electrodes respectively. The performances of conventional PSCs and inverted OSCs were measured using a calibrated air mass (AM) 1.5 G solar simulator (Oriel Sol3A Class AAA solar simulator, models 94043A, Newport Stratford, Inc., USA) with a light intensity of 100 mW/cm^2 adjusted using a standard PV reference cell (2 cm × 2 cm monocrystalline silicon solar cell, calibrated at NREL, Golden, CO) and a computer controlled Keithley 2400 (Keithley Instruments, Inc. USA) source measure unit. The EQE spectrum was measured using an Oriel IQE-200 (Newport Stratford, Inc., USA) equipped with a 250-W quartz tungsten halogen lamp as the light source and a monochromator, an optical chopper, a lock-in amplifier, and a calibrated silicon photodetector. While measuring the *J–V* curves, a black mask was used and only the effective area of the cell was exposed to light irradiation. DFT calculations at the B3LYP/6–31G(d,p) level were carried out on Gaussian 09. Electrochemical impedance spectroscopy (EIS) was measured with a VersaSTAT-3 (Princeton Applied Research, USA) work station with an ac signal of 15 mV in the frequency range of 1 Hz-1 MHz. The experimental data were simulated using commercial *Z*-view software to estimate the values for each component of the corresponding equivalent circuits. Alpha-step IQ surface profilometer USA with an accuracy of ±1 nm. AFM images were acquired with a XE-100 (Park system corp., Korea) in tapping mode. FE-SEM imaging and energy-dispersive X-ray spectroscopy (EDS) were performed on a S-4800 instrument (Hitachi, Japan) at an accelerating voltage of 15.0 kV. Focused-ion-beam (FIB)-SEM images were obtained on a Helios Nano Lab at an accelerating voltage of 2.0 kV. Water contact angles were carried out with a contact angle 101 measuring system (PSM Company). All

photoemission measurements were carried out in a PHI-5000 Versa Probe II (ULVAC-PHI, Inc. Japan) ultrahigh vacuum surface analysis system equipped with a He-discharge lamp (21.22 eV) and a monochromatic Al kα X-ray. All spectra were measured at a pressure of 1×10^{-6} Pa 2D-GIWAXS measurements were conducted at beamline 9A in the Pohang Accelerator Laboratory (Korea). By spin-coating under optimized fabricating condition, the 2D-GIWAXS samples were prepared onto a PEDOT:PSS/Si substrate. To permit for complete penetration of X-rays into the 2D-GIWAXS samples, the incidence angle (~0.12°) was used with a wavelength of 1.1179 °A. Time-resolved microwave conductivity (TRMC) evaluations were performed using ca. 9.1 GHz microwave as the probe and nanosecond laser (Continuum Inc., Surelite II with optical parametric oscillation, 5-8 ns pulse duration) at 500 nm (incident photon density: 1.3×10^{11} photons cm^{-2} $pulse^{-1}$) as the excitation. The photoconductivity transient $\Delta\sigma$ is converted to the product of the quantum efficiency (φ) and the sum of charge carrier mobilities, $\Sigma\mu$ ($=\mu_+ + \mu_-$) by $\varphi\Sigma\mu = \Delta\sigma\ (eI_0F_{light})^{-1}$, where e and F_{Light} are the unit charge of a single electron and a correction (or filling) factor, respectively. The hole transfer yield (η_{HT}) was evaluated by $\eta_{HT} = (\varphi\Sigma\mu - \varphi\Sigma\mu_{HTM})/\ \varphi\Sigma\mu$, where the $\varphi\Sigma\mu$ and $\varphi\Sigma\mu_{HTM}$ are the TRMC signals of quartz/mp-TiO_2/perovskite and quartz/mp-TiO_2/perovskite/HTM samples, respectively. The $\eta_{HT}(t)$ was normalized via $(\eta_{sat} - \eta_{HT}(t))/(\eta_{sat} - \eta_0)$, where η_0 and η_{sat} are the hole transfer yields at the pulse-end and saturated region, respectively, and further analyzed by stretched exponential function, $\exp(-(kt)^{\beta})$, where k and β are the hole transfer rate (s^{-1}) and power factor, respectively. All experiments were conducted at room temperature in air.

Fabrication and characterization of PSCs. Fluorine-doped tin oxide (FTO) glasses (Pilkington, TEC-8, 15Ω/sq) were cleaned with detergent, diluted water, and acetone and then sonicated with isopropyl alcohol (IPA) in an ultrasonic bath for 60 min then followed by UV-O_3

treatment for 20 min. The TiO_2 blocking layer (bl-TiO_2, ~ 40 nm, 0.15 M titanium diisopropoxide dis(acetylacetonate) (75 wt% in IPA) in 1-butanol was spin-coated on a FTO glass substrate at 2000 rpm for 20 sec, which was dried at 125 ^oC for 5 min. Further mesoporous TiO_2 (mp-TiO_2, ~ 200 nm) layer was deposited on the bl-TiO_2 by spin-coating the TiO_2 colloidal solution containing 3.5 g of TiO_2 paste (50 nm sized nanocrystalline TiO_2, terpineol, ethyl cellulose and lauric acid with a nominal ratio of 1.25:6:0.6:0.1 in wt%) diluted in 10 mL of anhydrous ethanol solution at ~2000 rpm for 20 sec, which was annealed at 550 ^oC for 1 h and then UV-O_3 was treated for 20 min. The substrate was further treated with 20 mM aqueous $TiCl_4$ solution at 90 ^oC for 10 min, cleaned with deionized water and then sintered at 500 ^oC for 30 min. PbI_2 (461 mg), CH_3NH_3I (159 mg) and DMSO (78 mg, molar ratio 1:1:1) was mixed in DMF solution (600 mg) at room temperature with stirring for 1 h in order to prepare a CH_3NH_3I•PbI_2•DMSO adduct solution. The completely dissolved solution was spin-coated on the mp-TiO_2 layer at 4000 rpm for 25 sec and 0.5 mL of diethyl ether was slowly dripped on the rotating substrate in 10 sec before the surface changed to be turbid caused by rapid vaporization of DMF. The transparent CH_3NH_3I•PbI_2•DMSO adduct film was heated at 65 ^oC for 1 min and 100 ^oC for 2 min in order to obtain a dense $CH_3NH_3PbI_3$ film (~ 400 nm). The 25 μL of spiro-OMeTAD solution, which was consisted of spiro-OMeTAD (72.3 mg), 4-tert-butylpyridine (28.8 μL) and lithium bis(trifluoromethanesulfonyl)imide (Li-TFSI, 17.5 μL) solution (520 mg Li-TSFI in 1 mL acetonitrile) in CB (1 mL) was spin-coated on the perovskite layer at 3000 rpm for 30 sec (~ 190 nm). The new polymers (10 mg/1 mL CB, ~35 nm) were spin-coated on perovskite layer at 2000 rpm for 30 sec. Finally, Ag (150 nm) electrode was deposited by using thermal evaporator at a constant evaporation rate of 0.03 nm/s. The active area of PSCs is 0.11 cm^2.

Fabrication and characterization of BHJ OSCs. The indium tin oxide (ITO) coated glass substrates that have been used for fabrication were ultrasonically cleaned with detergent, water, acetone, and IPA. Electron transporting layer ZnO was prepared using standard sol-gel procedure, by dissolving zinc acetate dihydrate ($Zn(O_2CCH_3)_2 \cdot (H_2O)_2$, 99.9%, 1 g) and ethanolamine ($HOCH_2CH_2NH_2$, 99.5%, 0.28 g) in anhydrous 2-methoxy ethanol ($CH_3OCH_2CH_2OH$, > 99.8%, 10 mL) under vigorous stirring for more than 24 h to allow the hydrolysis reaction and aging to proceed. A filtered ZnO soluiton was applied by spin-coating at 4000 rpm for 40 sec and baking for 10 min at 200 °C in air, and then the devices were transferred to a glove box. Then, optimized donor:acceptor (P1-P3:$PC_{71}BM$) ratio 1:1 (w/w) in CB with 2.0 vol% dipehenyl ether solutions were spin-cast onto an ITO/ZnO substrate at 3000 rpm for 40 sec. And then, the solutions were filtered by a 0.45-μm polytetrafluoroethylene syringe filter. The optimized thickness of active layer films was found to be 100 ± 5 nm. These blend layers were treated with 1-butanol at 3000 rpm for 40 sec and drying for 30 min in a glove box. And then, PEDOT:PSS (Clevios P VP AI 4083), diluted using IPA with a ratio of PEDOT:PSS:IPA of 1:10 layer was spin casted on top of active layer. The devices were then moved in an evaporation chamber and held under high vacuum (< 10^{-6} Torr) for more than 2 h and 120 nm of Ag was thermally deposited. The active area of the fabricated devices about 0.11 cm^2.

Hole mobility. Charge carrier mobility measurements of P1-P3, P1-P3:$PC_{71}BM$ hole mobilities, P1-P3:$PC_{71}BM$ electron mobilities was performed with a device structure ITO/PEDOT:PSS/Polymer (P1-P3)/MoO_3/Al, ITO/PEDOT:PSS/P1-P3:$PC_{71}BM$/MoO_3/Al and ITO/ZnO/P1-P3:$PC_{71}BM$/LiF/Al, respectively. The mobility determined by fitting the dark *J–V* curve into the SCLC model (based on the equation derived by the Mott-Gurney law).

$$J = \left(\frac{9}{8}\right) \varepsilon_r \varepsilon_0 \mu \left(\frac{V^2}{L^3}\right)$$

Where, ε_r is the dielectric constant of polymer, ε_0 is vacuum permittivity, L is thickness of the active layer, μ is mobility and V is voltage drop across the device.

Microwave assisted polymer synthesis.

P1-P3 were synthesized by applying microwave-assisted Stille polymerization (**Scheme S1**). The general procedure for the synthesis of polymer P1 is as follows: To a 10 mL microwave tube, compound D1 (0.27 mmol), and A (0.27 mmol), $Pd_2(dba)_3$ (5.4 mg, 2 mol%), and (*o*-tol)$_3$P (16 mg, 16 mol%) were dissolved in CB (2 mL). The reaction mixture was purged with N_2 for 15 min. The microwave tube was placed into the reactor and heated to 150 $^{\circ}$C for 3 h. The resulted precipitate was purified by soxhlet extraction method using methanol, hexane, acetone, and chloroform. The chloroform fraction was evaporated to yield P1.

Poly[4,8-bis(2-(4-(2-ethylhexyloxy)phenyl)-5-thienyl)benzo[1,2-b:4,5-b']dithiophene-alt-1,3-bis(4-octylthien-2-yl)-5-(2-ethylhexyl)thieno[3,4-c]pyrrole-4,6-dione] (P1). Yield: 55%. ^{1}H NMR (300 MHz, $CDCl_3$): δ (ppm). 7.25-7.59 (br, 10H), 6.90 (br, 6H), 3.85 (br, 4H), 3.54 (br, 2H), 2.82-2.92 (br, 4H), 1.70-1.74 (m, 3H), 1.30-1.55 (m, 48H), 0.90 (m, 24H). Anal. Calcd: C, 71.29; H, 7.34; N, 0.99. Found C, 70.98; H, 7.22; N, 0.89.

Poly[4,8-bis(2-(4-(2-ethylhexyloxy)3-fluorophenyl)-5-thienyl)benzo[1,2-b:4,5-b'] dithiophene-alt-1,3-bis(4-octylthien-2-yl)-5-(2-ethylhexyl)thieno[3,4-c]pyrrole-4,6-dione] (P2). Yield: 67%. ^{1}H NMR (300 MHz, $CDCl_3$): δ (ppm). 7.27-7.58 (br, 8H), 6.88 (br, 6H), 3.84 (br, 4H), 3.52 (br, 2H), 2.02-2.93 (br, 4H), 1.70-1.74 (m, 3H), 1.29-1.55 (m, 48H), 0.89 (m, 24H). Anal. Calcd: C, 69.52; H, 7.02; N, 0.97. Found C, 69.42; H, 6.96; N, 0.99.

Poly[4,8-bis(2-(4-(2-ethylhexyloxy)3,5-fluorophenyl)-5-thienyl)benzo[1,2-b:4,5-b']dithiophene-alt-1,3-bis(4-octylthien-2-yl)-5-(2-ethylhexyl)thieno[3,4-c]pyrrole-4,6-dione] (P3). Yield: 68%. ^{1}H NMR (300 MH_Z, $CDCl_3$): δ (ppm). 7.28-7.57 (br, 6H), 6.86 (br, 6H), 3.85 (br, 4H), 3.50 (br, 2H), 2.02-2.91 (br, 4H), 1.70-1.74 (m, 3H), 1.29-1.54 (m, 48H), 0.89 (m, 24H). Anal. Calcd for $C_{84}H_{99}F_4NO_4S_7$: C, 67.84; H, 6.71; N, 0.94. Found C, 67.88; H, 6.54; N. 0.96.

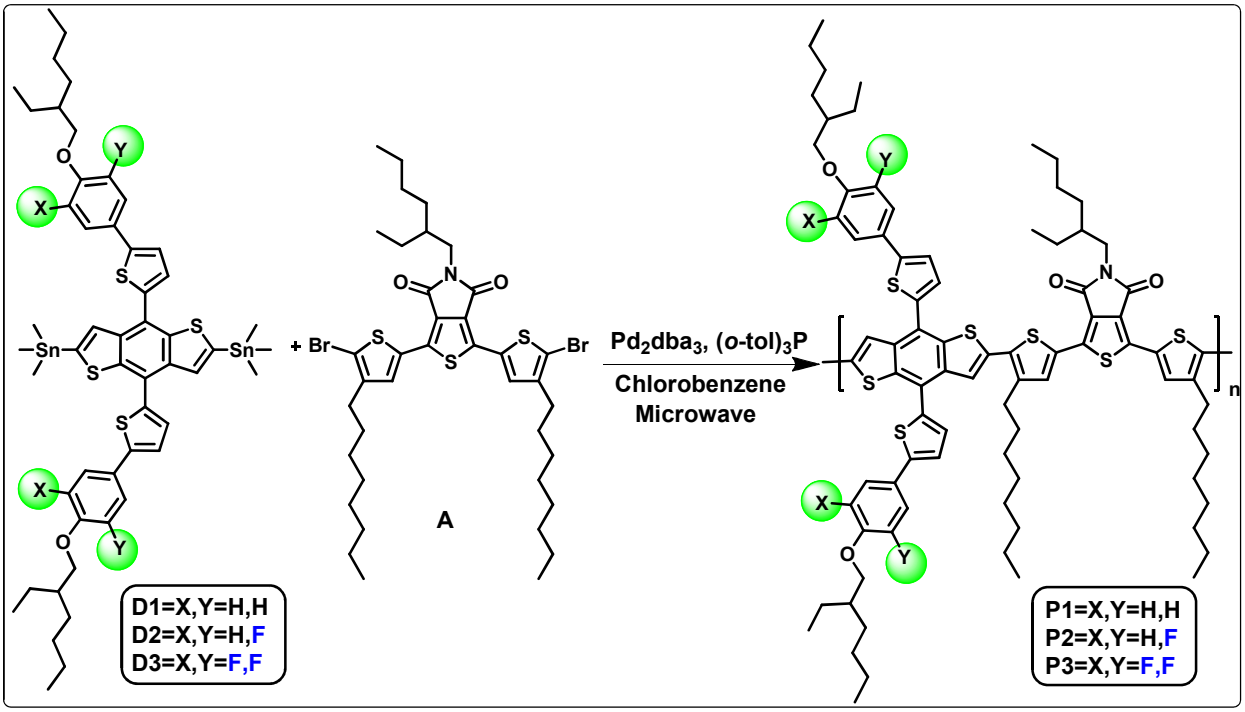

Scheme S1. Synthetic route for polymers.

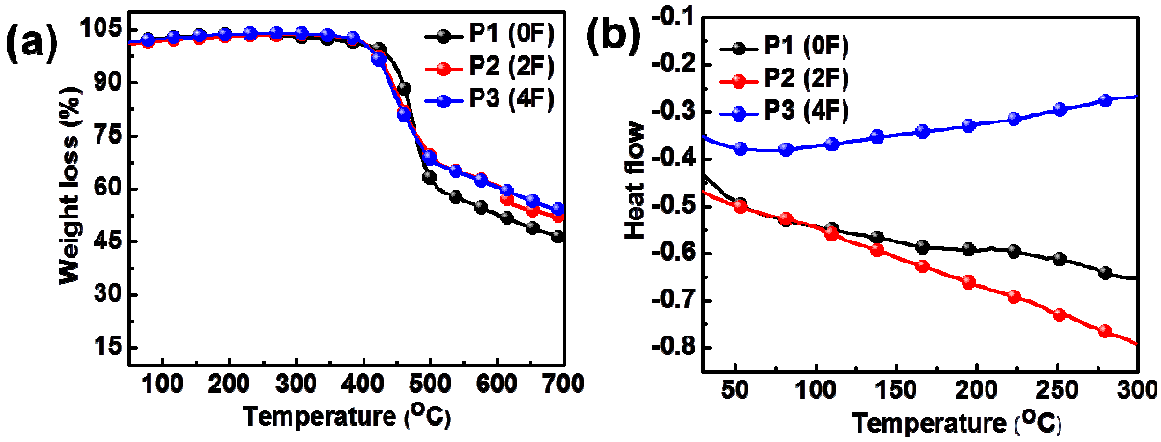

Figure S1. (a) TGA curves of P1-P3. (b) DSC curves of P1-P3.

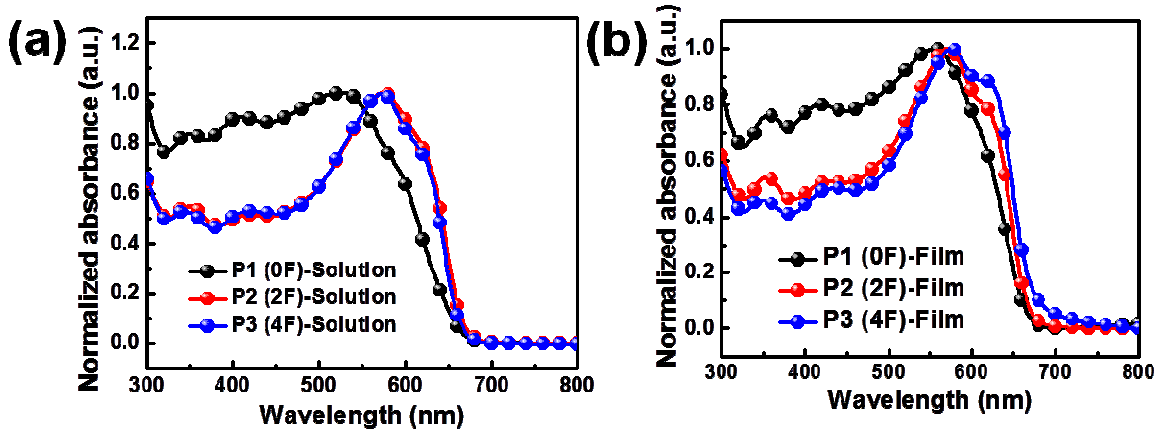

Figure S2. Normalized UV-visible absorption spectra of P1-P3 in (a) solution and (b) film state.

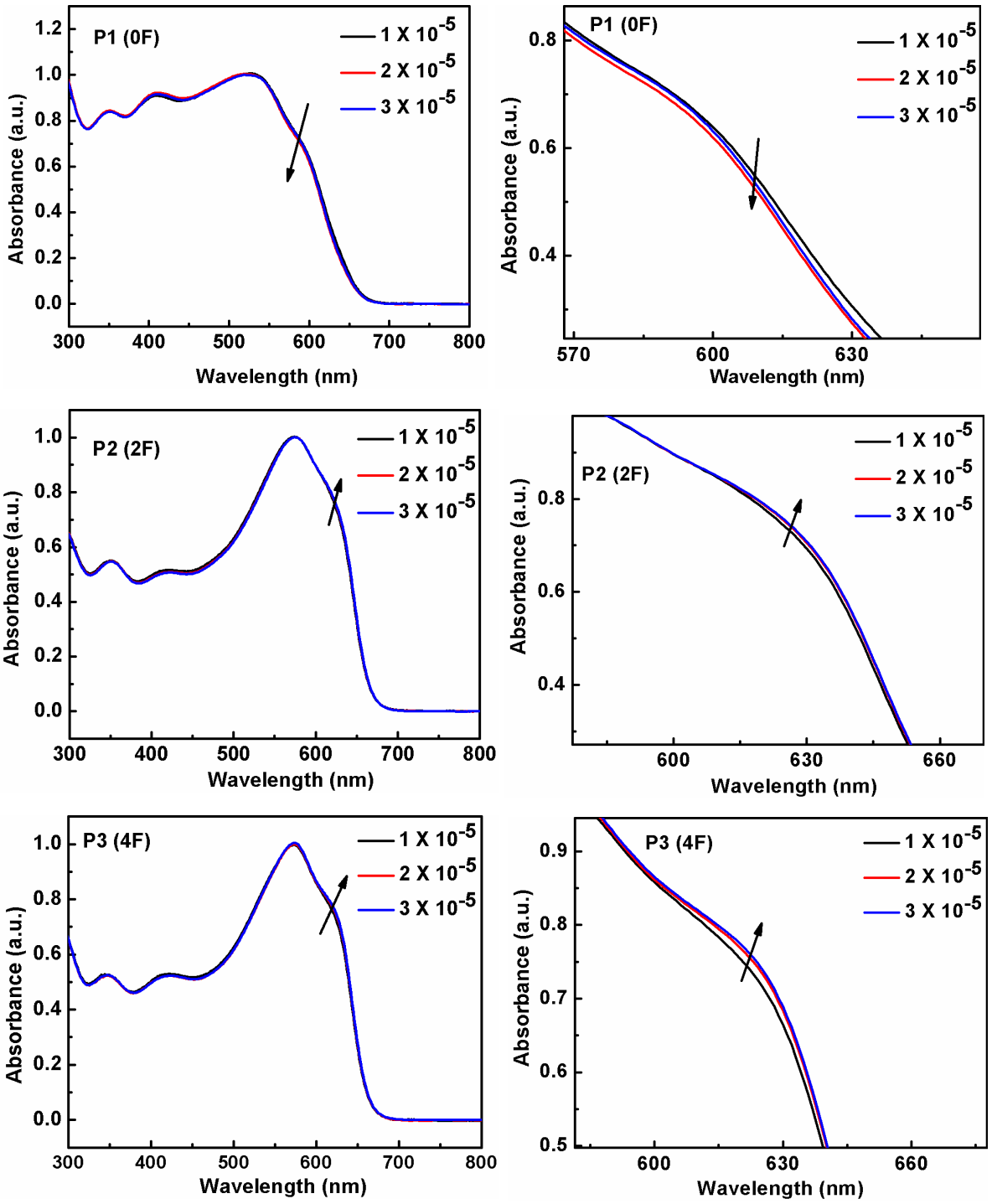

Figure S3. Concentration dependent UV-visible absorption spectra of P1-P3.

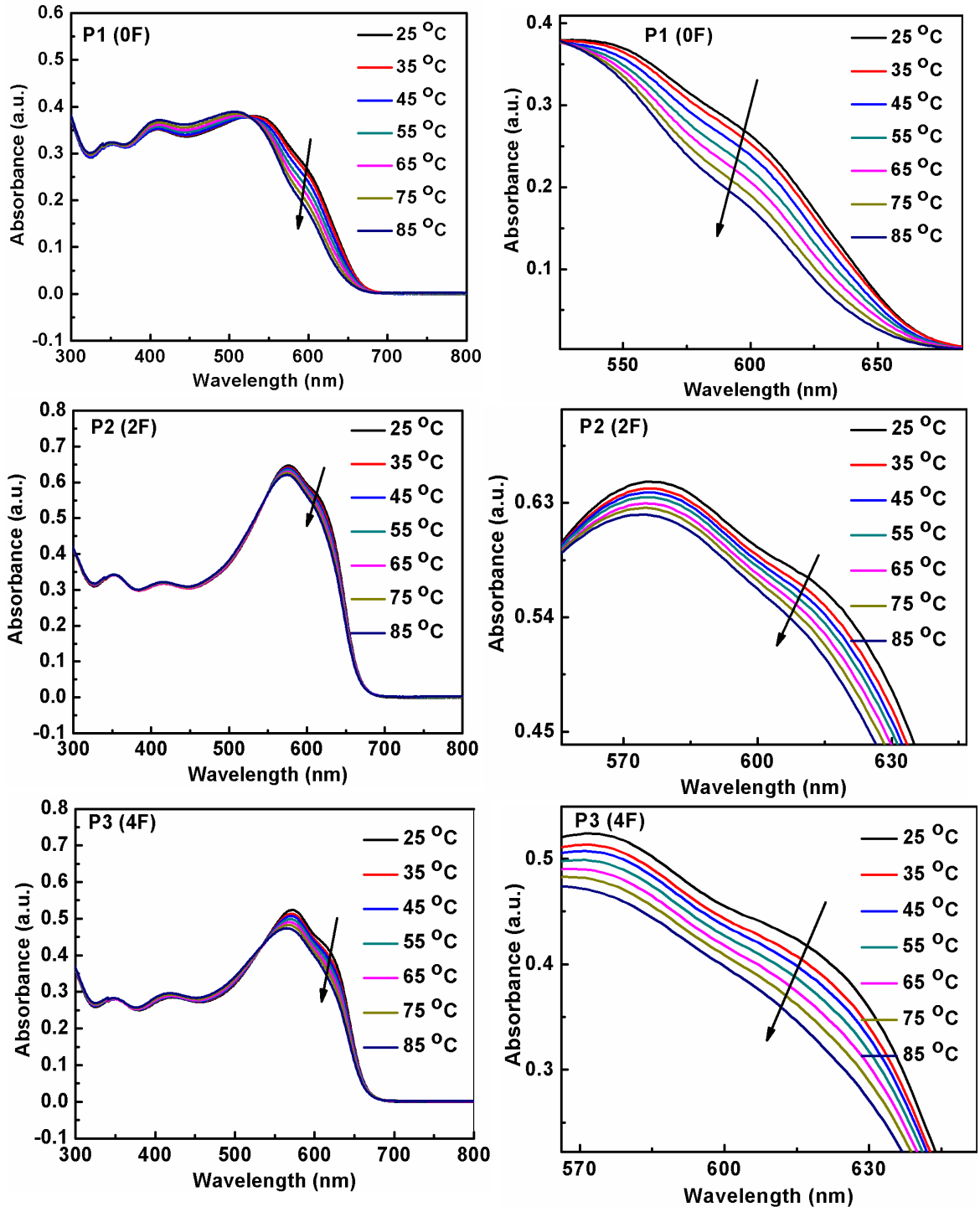

Figure S4. Temperature dependent UV-visible absorption spectra of P1-P3.

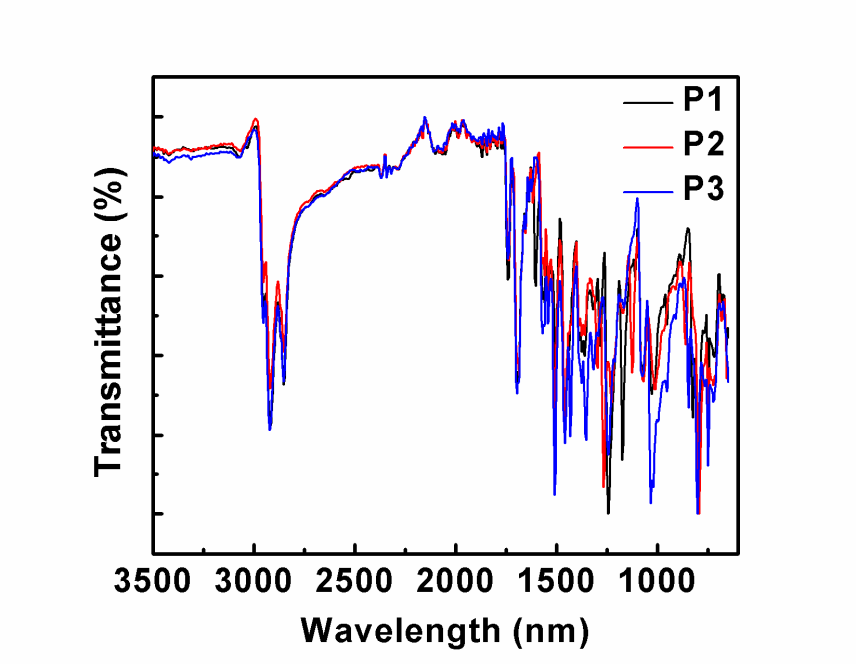

Figure S5. FTIR-spectra of P1-P3.

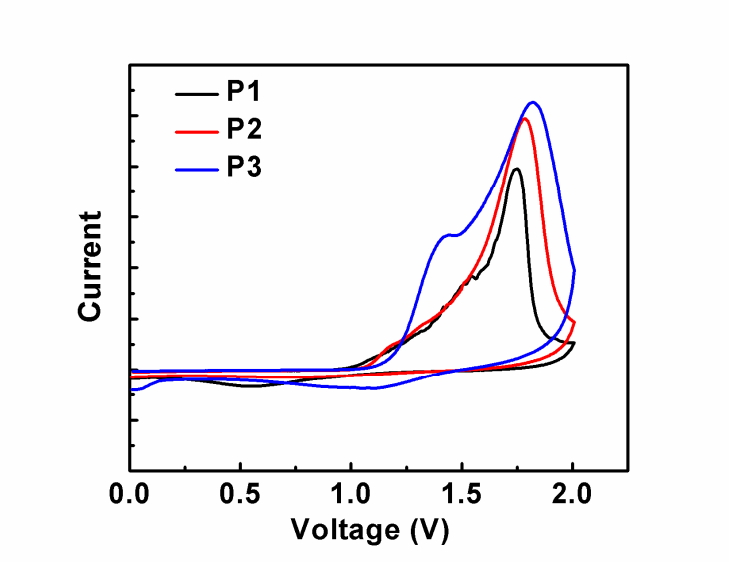

Figure S6. Cyclic voltammograms of P1-P3.

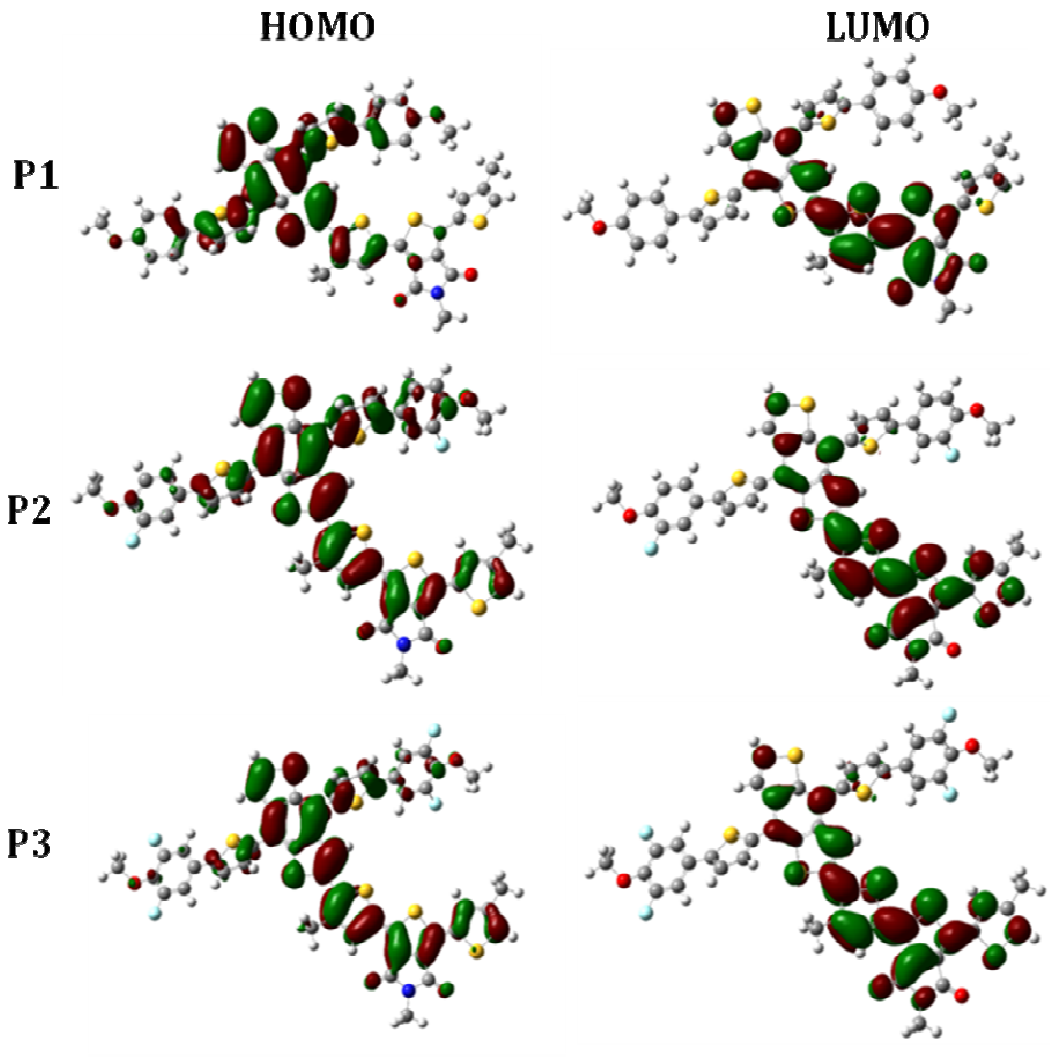

Figure S7. DFT calculated HOMOs and LUMOs of P1-P3.

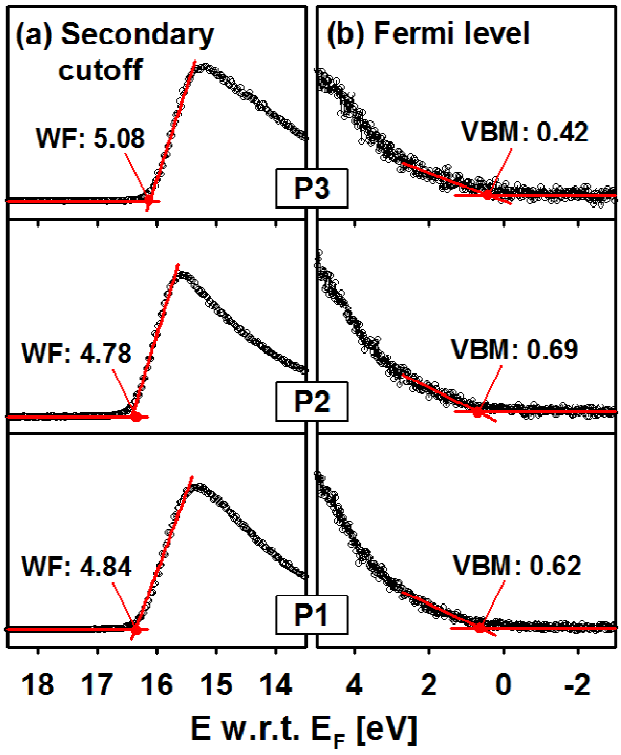

Figure S8. UPS spectra of P1-P3, determination of (a) work function (WF) of P1-P3 and (b) valence band maximum (VBM) of P1-P3.

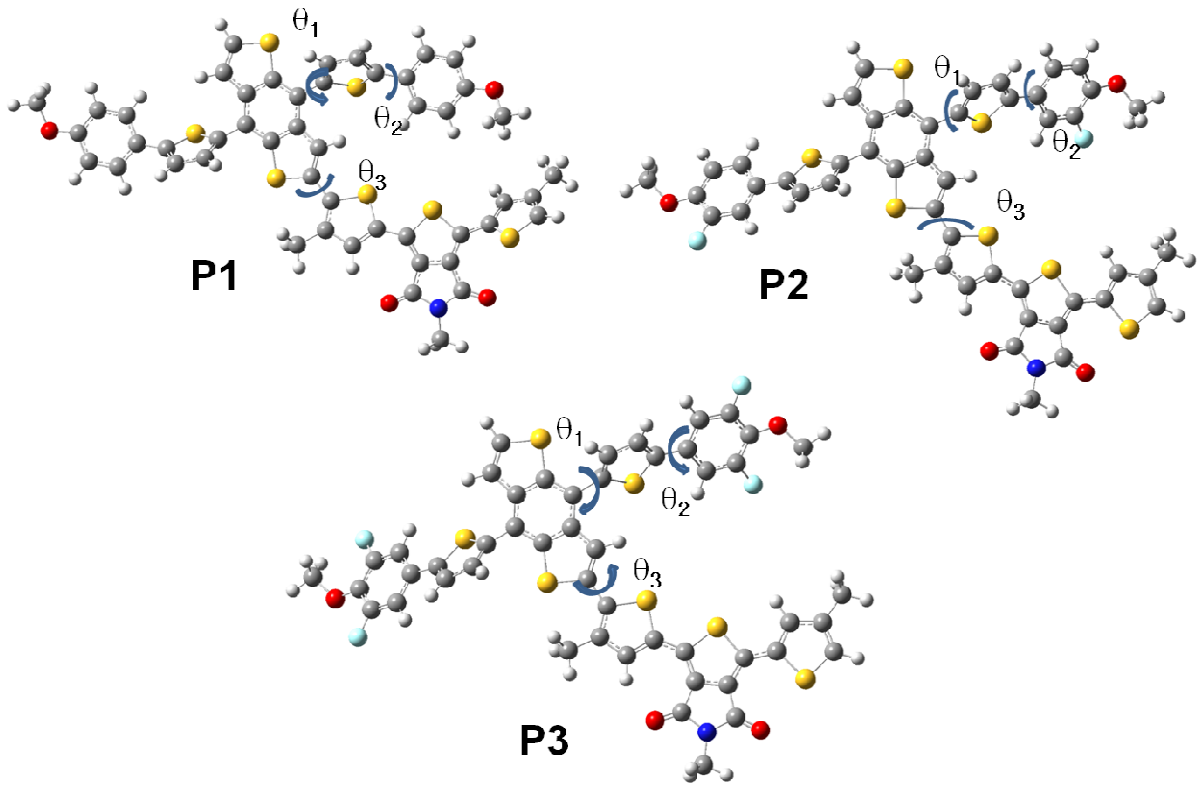

Figure S9. Dihedral angles of P1-P3.

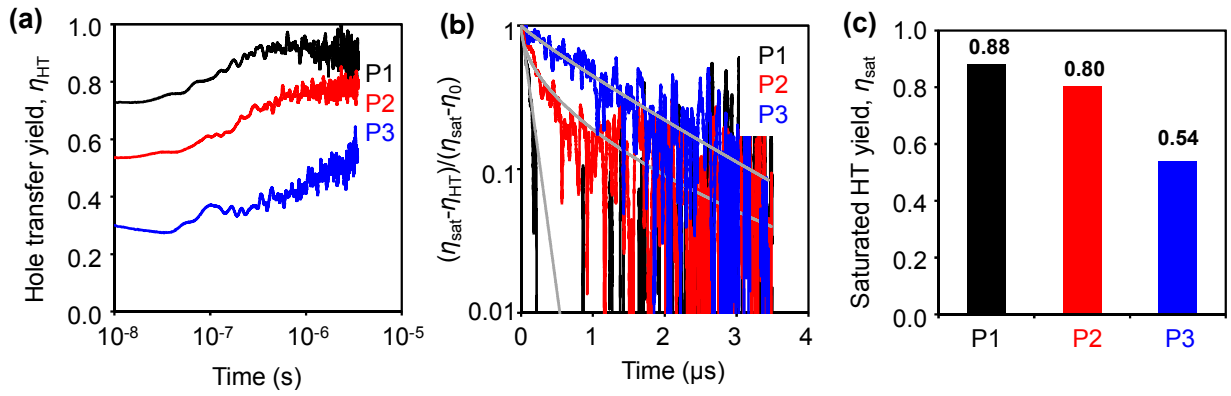

Figure S10. (a) Time-dependent hole transfer yields from perovskite to P1-P3 evaluated by flash-photolysis TRMC (λ_{ex} = 500 nm). (b) Normalized profiles of hole transfer yields. The gray lines are fitting curves of stretched exponential function, $\exp(-(kt)^{\beta})$. (c) Saturated hole transfer yield, η_{sat}, of P1-P3.

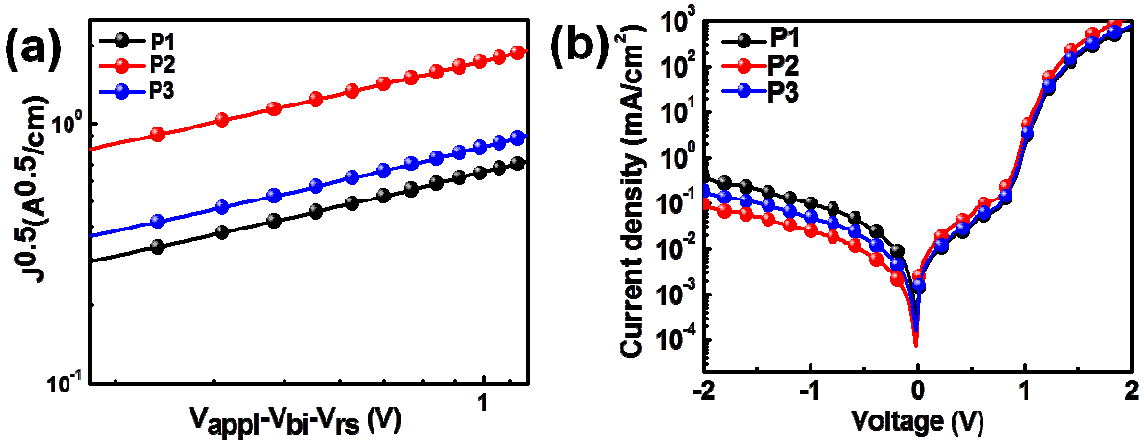

Figure S11. (a) SCLC hole mobility of P1-P3. (b) Dark *J-V* curves of P1-P3 based PSCs.

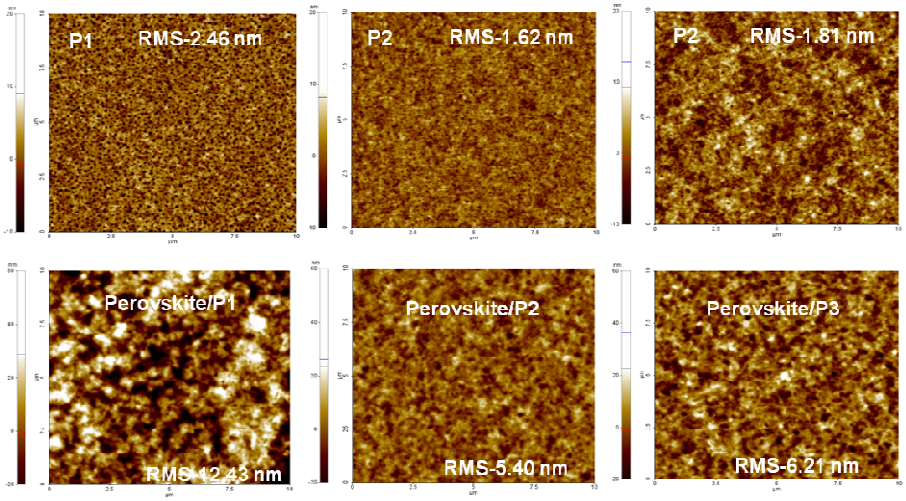

Figure S12. AFM images of pristine P1-P3 and perovskite:P1, perovskite:P2 and perovskite:P3 films.

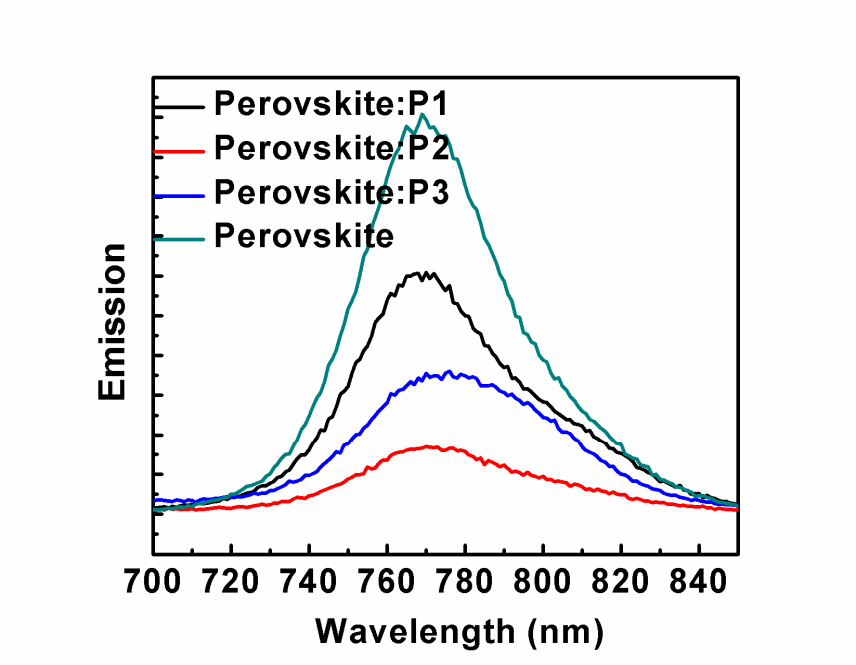

Figure S13. PL spectra of perovskite, perovskite:P1, perovskite:P2 and perovskite:P3.

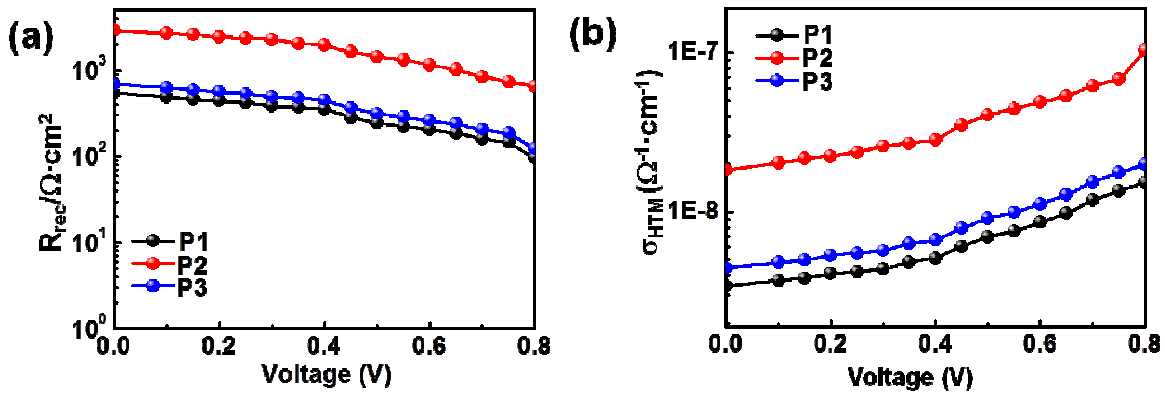

Figure S14. (a) Recombination resistance (R_{rec}). (b) Hole conductivities (σ_{HTM}) of the HTMs (P1-P3) extracted from the EIS measurements.

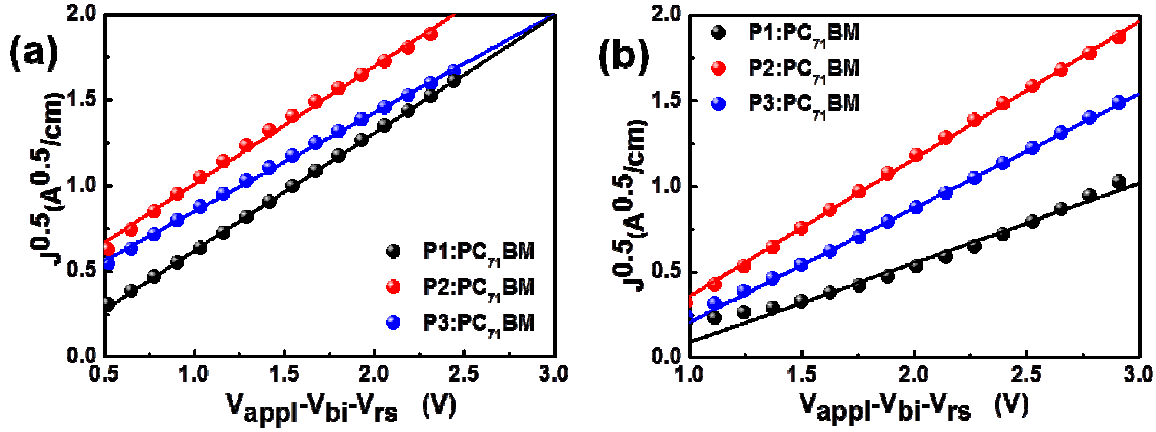

Figure S15. SCLC (a) hole mobilities and (b) electron mobilities of P1-P3:$PC_{71}BM$ optimized blends.

Table S1. Preliminary Characteristics of the P1-P3.

Polymer	M_n/PDI (kDa)[a]	T_d (°C)[b]	Solution λ_{max} (nm)	Film λ_{max} (nm)	E_g^{opt} (eV)[c]	HOMO (eV)[d]	LUMO (eV)[e]	HOMO (eV)[f]	LUMO (eV)[e]
P1	17/1.82	446	526	554	1.82	-5.41	-3.59	-4.84	-3.02
P2	58/2.21	429	574	568, 616	1.82	-5.43	-3.61	-4.78	-2.96
P3	38/1.50	426	573	569, 616	1.82	-5.50	-3.68	-5.08	-3.26

[a]Determined by GPC using THF as the eluent at 25 °C. [b]Measured by thermo gravimetric analysis. [c]UV-vis absorption onsets in the polymer film. [d]Measured by cyclic voltammetry. [e]LUMO = HOMO + E_g^{opt}. [f] Calculated from UPS.

Table S2. Dihedral Angle Study of P1-P3.

Polymer	θ1 (degree)	θ2 (degree)	θ3 (degree)
P1	51.49	-27.88	-24.28
P2	52.11	-26.92	-19.39
P3	53.33	-24.41	-17.70

Table S3. Dopant-Free Polymer HTMs in PSCs.

Polymer	PCE Max (%)	PCE Avg (%)	Role	Reference
TTB–TTQ	6.2	-	Only HTM	1
PBDTTT-C	9.95	9.32	Only HTM	2
PCBTDPP	5.5	-	Only HTM	3
P3HT	10.4	10.4	Only HTM	4
PTB-DCB21	8.7	6.0	Only HTM	5
PTB7	7.5	-	Only HTM	6
TB1	6.0	-	Only HTM	6
P1	6.64	-	Only HTM	7
PEDOT	14.5	-	Only HTM	8
P3HT	13.7	-	Only HTM	9
P	10.80	10.0	Only HTM	10
pBBTa-BDT2	14.5	12.57	Only HTM	11
V873	12.29	-	Only HTM	12
PEDOT	13.1	-	Only HTM	13
RCP	17.3 (Reverse) 12.6 (Forward)	14.95	Only HTM	14
P3	17.28 (Reverse) 17.20 (Forward)	17.24	HTM and Photoactive donor (PCE=8.26%)	15
P2 (2F)	14.94 (Reverse) 14.06 (Forward)	14.50	HTM & Photo active Donor (P2=7.93%, *Voc*=0.82V; P3=7.43%, *Voc*=1.00 V)	Present Work

Table S4. Summary of Analysis on the Hole Transfer Yields.

Polymer	η_0	η_{sat}	k (s^{-1})	β
P1	0.73	0.88	8.5×10^6	1.00
P2	0.53	0.80	2.6×10^6	0.53
P3	0.32	0.54	7.9×10^5	0.91

Table S5. SCLC Mobilities of Optimized P1-P3:$PC_{71}BM$ blends.

Blend	Hole mobility (μ_h) ($cm^2V^{-1}s^{-1}$)	Electron mobility (μ_e) ($cm^2V^{-1}s^{-1}$)	Charge balance (μ_h/μ_e)
P1:$PC_{71}BM$	8.40×10^{-4}	2.35×10^{-4}	3.57
P2:$PC_{71}BM$	1.81×10^{-3}	9.23×10^{-4}	1.96
P3:$PC_{71}BM$	1.37×10^{-3}	5.63×10^{-4}	2.43

REFERENCES

(1) Kim, G.-W.; Kim, J.; Lee, G.-Y.; Kang, G.; Lee, J.; Park, T. A Strategy to Design a Donor–π–Acceptor Polymeric Hole Conductor for an Efficient Perovskite Solar Cell. *Adv. Energy Mater.* **2015**, *5*, 1500471.

(2) Chen, W.; Bao, X.; Zhu, Q.; Zhu, D.; Qiu, M.; Sun, M.; Yang, R. Simple Planar Perovskite Solar Cells with a Dopant-Free Benzodithiophene Conjugated Polymer as Hole Transporting Material. *J. Mater. Chem. C* **2015**, *3*, 10070-10073.

(3) Cai, B.; Xing, Y.; Yang, Z.; Zhang, W.-H.; Qiu, J. High Performance Hybrid Solar Cells Sensitized by Organolead Halide Perovskites. *Energy Environ. Sci.* **2013**, *6*, 1480-1485.

(4) Conings, B.; Baeten, L.; De Dobbelaere , C.; D'Haen, J.; Manca, J.; Boyen, H.-G. Perovskite-Based Hybrid Solar Cells Exceeding 10% Efficiency with High Reproducibility Using a Thin Film Sandwich Approach. *Adv. Mater.* **2014**, *26*, 2041-2046.

(5) Lee, J.-W.; Park, S.; Ko, M. J.; Son, H. J.; Park, N.-G. Enhancement of the Photovoltaic Performance of $CH_3NH_3PbI_3$ Perovskite Solar Cells through a Dichlorobenzene-Functionalized Hole-Transporting Material. *Chem.Phys.Chem* **2014**, *15*, 2595-2603.

(6) Marin-Beloqui, J. M.; Hernández, J. P.; Palomares, E. Photo-Induced Charge Recombination Kinetics in $MAPbI_3$-xClx Perovskite-Like Solar Cells Using Low Band-Gap Polymers as Hole Conductors. *Chem. Commun.* **2014**, *50*, 14566-14569.

(7) Nagarjuna , P.; Narayanaswamy, K.; Swetha, T.; Hanumantha Rao, G.; Singh, S. P.; Sharma, G. D. $CH_3NH_3PbI_3$ Perovskite Sensitized Solar Cells Using a D-A Copolymer as Hole transport Material. *Electrochim. Acta* **2015**, *151*, 21-26.

(8) Liu, J.; Pathak, S.; Stergiopoulos, T.; Leijtens, T.; Wojciechowski, K.; Schumann, S.; Busies, N. K.; Snaith, H. J. Employing PEDOT as the p-Type Charge Collection Layer in Regular Organic–Inorganic Perovskite Solar Cells. *J. Phys. Chem. Lett.* **2015**, *6*, 1666-1673.

(9) Abbas, H. A.; Kottokkaran, R.; Ganapathy, B.; Samiee, M.; Zhang, L.; Kitahara, A.; Noack, M.; Dalal, V. L. High Efficiency Sequentially Vapor Grown n-i-p $CH_3NH_3PbI_3$ Perovskite Solar Cells with Undoped P3HT as p-Type Heterojunction Layer. *APL Mater.* **2015**, *3*, 016105.

(10) Zhu, Q.; Bao, X.; Yu, J.; Zhu, D.; Qiu, M.; Yang, R.; Dong, L. Compact Layer Free Perovskite Solar Cells with a High-Mobility Hole-Transporting Layer. *ACS Appl. Mater. Interfaces* **2016**, *8*, 2652-2657.

(11) Liao, H.-C.; Dexter Tam, T. L.; Guo, P.; Wu, Y.; Manley, E. F.; Huang, W.; Zhou, N.; Soe, C. M. M.; Wang, B.; Wasielewski, M. R.; Chen, L. X.; Kanatzidis, M. G.; Facchetti, A.; Chang, R. P. H.; Marks, T. J. Dopant-Free Hole Transporting Polymers for High Efficiency Environmentally Stable Perovskite Solar Cells. *Adv. Energy Mater.* **2016**, *6*, 1600502.

(12) Matsui, T.; Petrikyte, I.; Malinauskas, T.; Domanski, K.; Daskeviciene, M.; Steponaitis, M.; Gratia, P.; Tress, W.; Correa-Baena, J.-P.; Abate, A.; Hagfeldt, A.; Gratzel, M.; Nazeeruddin, M. K.; Getautis, V.; Saliba, M. Additive-Free Transparent Triarylamine-Based Polymeric Hole-Transport Materials for Stable Perovskite Solar Cells. *ChemSusChem* **2016**, *9*, 2567-2571.

(13) Li, Y.; Liu, M.; Li, Y.; Yuan, K.; Xu, L.; Yu, W.; Chen, R.; Qiu, X.; Yip, H.-L. Poly(3,4-Ethylenedioxythiophene): Methylnaphthalene Sulfonate Formaldehyde Condensate: The Effect of Work Function and Structural Homogeneity on Hole Injection/Extraction Properties. *Adv. Energy Mater.* **2017**, *7*, 1601499.

(14) Kim, G.-W.; Kang, G.; Kim, J.; Lee, G.-Y.; Kim, H. I.; Pyeon, L.; Lee, J.; Park, T. Dopant-Free Polymeric Hole Transport Materials for Highly Efficient and Stable Perovskite Solar Cells. *Energy Environ. Sci.* **2016**, *9*, 2326-2333.

(15) Kranthiraja, K.; Gunasekar, K.; Kim, H.; Cho, A.-N.; Park, N.-G.; Kim, S.; Kim, B. J.; Nishikubo, R.; Saeki, A.; Song, M.; Jin, S.-H. High-Performance Long-Term-Stable Dopant-Free Perovskite Solar Cells and Additive-Free Organic Solar Cells by Employing Newly Designed Multirole π-Conjugated Polymers. *Adv. Mater.* **2017**, *29*, 170083.